



Original Research

Hydrogen absorption properties of amorphous $(\text{Ni}_{0.6}\text{Nb}_{0.4-y}\text{Ta}_y)_{100-x}\text{Zr}_x$ membranesO. Palumbo^a, F. Trequattrini^{a,b}, N. Pal^c, M. Hulyalkar^c, S. Sarker^c, D. Chandra^c, T. Flanagan^d, M. Dolan^e, A. Paolone^{a,*}^a CNR-ISC, U.O.S. La Sapienza, Piazzale A. Moro 5, 00185 Roma, Italy^b Department of Physics, Sapienza University of Rome, Piazzale A. Moro 5, 00185 Roma, Italy^c Department of Chemical and Materials Engineering, University of Nevada, Reno, NV 89557, USA^d Department of Chemistry, University of Vermont, Burlington, VT 05405, USA^e CSIRO, QCAT, Energy, 1 Technology Court, Pullenvale, QLD 4069, Australia

ARTICLE INFO

Keywords:

Amorphous Ni based alloy ribbons
High temperature X-ray diffraction
DTA
Activation energy
Crystallization temperature
Hydrogen solubility

ABSTRACT

Ni based amorphous materials have great potential as hydrogen purification membranes. In the present work the melt spun $(\text{Ni}_{0.6}\text{Nb}_{0.4-y}\text{Ta}_y)_{100-x}\text{Zr}_x$ with $y=0, 0.1$ and $x=20, 30$ was studied. The result of X-ray diffraction spectra of the ribbons showed an amorphous nature of the alloys. Heating these ribbons below $T < 400$ °C, even in a hydrogen atmosphere (1–10 bar), the amorphous structure was retained. The crystallization process was characterized by differential thermal analysis and the activation energy of such process was obtained. The hydrogen absorption properties of the samples in their amorphous state were studied by the volumetric method, and the results showed that the addition of Ta did not significantly influence the absorption properties, a clear change of the hydrogen solubility was observed with the variation of the Zr content. The values of the hydrogenation enthalpy changed from ~ 37 kJ/mol for $x=30$ to ~ 9 kJ/mol for $x=20$. The analysis of the volumetric data provides the indications about the hydrogen occupation sites during hydrogenation, suggesting that at the beginning of the absorption process the deepest energy levels are occupied, while only shallower energy levels are available at higher hydrogen content, with the available interstitial sites forming a continuum of energy levels.

1. Introduction

Novel Ni-Nb-Zr amorphous alloys are potential candidates as hydrogen permeation membranes to separate H_2 from CO_2 and other gases obtained from water shift reaction of coal-derived syngas [1]. Typically, commercial Pd/Pd-23Ag (at%) crystalline membranes are widely used for this purpose, but due to the high cost of Pd, replacement with inexpensive metals/alloys is necessary. In this framework, the amorphous alloys formed from a combination of Ni and one or more early transition metals show great promise for this application [1]. In particular, the hydrogen permeability of $(\text{Ni}_{0.6}\text{Nb}_{0.4})_{80}\text{Zr}_{20}$ and $(\text{Ni}_{0.6}\text{Nb}_{0.4})_{70}\text{Zr}_{30}$ membrane were 8.3×10^{-9} and $1.4 \times 10^{-8} \text{ mol m}^{-1} \text{ s}^{-1} \text{ Pa}^{-0.5}$ measured in pure hydrogen at 400 and 450 °C, respectively [2]. These values are comparable to those measured for pure Pd or Pd-23%Ag ($1-2 \times 10^8 \text{ mol m}^{-1} \text{ s}^{-1} \text{ Pa}^{-0.5}$ at 450 °C). The addition of other alloying metals in the Ni-Nb-Zr systems, such as Ta, Hf or Co, has been exploited in order to find possible higher

hydrogen permeation values or a better resistance to embrittlement [1]. Previous studies reported that the addition of Ta in Ni-Nb-Zr amorphous ribbon increases the devitrification temperature associated with decrease in embrittlement [3,4]. Moreover, it has been previously reported that with the addition of Ta, permeability undergoes only a moderate decrease: for example $(\text{Ni}_{0.6}\text{Nb}_{0.3}\text{Ta}_{0.1})_{80}\text{Zr}_{20}$ and $(\text{Ni}_{0.6}\text{Nb}_{0.3}\text{Ta}_{0.1})_{70}\text{Zr}_{30}$ exhibit permeability as 3.8×10^{-9} and $1.2 \times 10^{-8} \text{ mol m}^{-1} \text{ s}^{-1} \text{ Pa}^{-0.5}$ respectively at 450 °C [2]. However, in Ta added Ni-Nb-Zr alloys the permeability performances degrade as a function of time more slowly than in Ta-free membranes, possibly due to the stabilizing effect of Ta [2]. Therefore, the Ta containing alloys seem to have some advantages in comparison with Ta-free membranes.

The permeability of the amorphous membranes is the key parameter for their potential use in the production of ultrapure hydrogen; however, one should also consider that permeability is strictly linked to hydrogen solubility. First of all, it must be considered that during the permeation tests and the application as purification membranes, these

Peer review under responsibility of Chinese Materials Research Society.

* Corresponding author.

E-mail address: annalisa.paolone@roma1.infn.it (A. Paolone).<http://dx.doi.org/10.1016/j.pnsc.2017.01.002>

Received 3 November 2016; Accepted 30 November 2016

Available online 28 January 2017

1002-0071/© 2017 Chinese Materials Research Society. Published by Elsevier B.V.

This is an open access article under the CC BY-NC-ND license (<http://creativecommons.org/licenses/by-nc-nd/4.0/>).

amorphous materials undergo hydrogenation. Moreover, the knowledge of the hydrogenation properties is fundamental, since the formation of hydrides under certain operation conditions can lead to eventual failure of the membrane because of increased brittleness, and indeed it is a well known limitation of the Pd-based membranes [1]. Finally, solubility and permeability can be obtained one from the other mathematically, as the hydrogen flux through a membrane is linked to the shape of the pressure composition isothermal curves of the material [3].

Some previous studies on hydrogen solubility on membranes for hydrogen purification are available. Pd and Pd-Ag alloys with various contents of Ag were investigated by Flanagan et al., by Hara et al. and by Serra et al. [4–6]. A hydrogenation enthalpy of ~40 kJ/mol is reported [4–6]. The hydrogen solubility in other alloys containing Pd, such as Pd-V and Pd-M-Al (M= Rh, Ni, Pt, Cr, Ag), was investigated by Alimov et al. and by Wang et al. [7,8].

Many studies of the solubility of hydrogen in membranes for hydrogen purification concern vanadium based alloys, as V possesses one of the highest hydrogen diffusion coefficients. Binary, ternary and even quaternary V alloys were studied [9–14]. In one case a semi-empirical methodology for predicting the permeability and solubility of hydrogen in metallic alloys was proposed and compared with experiments [13].

Only a few reports about the solubility of hydrogen in amorphous membranes based on Ni, Nb and Zr are available [15,16]. Hao et al. reported pressure-composition curves measured at 573 K for $\text{Ni}_{60}\text{Nb}_{40}$, $(\text{Ni}_{0.6}\text{Nb}_{0.4})_{50}\text{Zr}_{50}$ and $(\text{Ni}_{0.6}\text{Nb}_{0.4})_{70}\text{Zr}_{30}$ [16]. The hydrogen content increases as the Zr content increases, reaching 1.1 mass% for $p \approx 0.6$ MPa [16]. Also Yamaura et al. showed a pressure-composition curve of $(\text{Ni}_{0.6}\text{Nb}_{0.4})_{70}\text{Zr}_{30}$ measured at 573 K, and, moreover, introduced methods combining density functional theory calculations and statistical mechanics to make predictions of the properties of interstitial H in amorphous metals [15].

However, to the best of our knowledge, a systematic investigation of the hydrogen absorption and formation enthalpies of $(\text{Ni}_{0.6}\text{Nb}_{0.4-y}\text{Ta}_y)_{100-x}\text{Zr}_x$ materials is still missing. In order to fill the lack of such information, in this study we measured the activation energies for crystallization of two Ta containing membranes by differential thermal analysis (TGA-DTA) and we also measured the hydrogen absorption properties of four $(\text{Ni}_{0.6}\text{Nb}_{0.4-y}\text{Ta}_y)_{100-x}\text{Zr}_x$ ribbons with $y=0, 0.1$ and $x=20, 30$ by volumetric method. The absorption data also provided indications about the hydrogen occupancy in the membrane, which is one of the controlling parameters for the hydrogen permeation through the bulk of the alloy membranes.

2. Materials and methods

The alloy buttons of $(\text{Ni}_{0.6}\text{Nb}_{0.4-y}\text{Ta}_y)_{100-x}\text{Zr}_x$ ($x=20$ or 30 ; $y=0$ or 0.1 compositions) were prepared by arc melting in a purified argon atmosphere at AMES Laboratory Iowa, USA. A melt spinning apparatus was used to fabricate these glassy membranes at the CSIRO laboratory, Brisbane, Australia. Typically the amorphous ribbons were ~30–70 μm thick and 30 mm wide [2,17]. In the paper we will use the following labels to indicate the four samples here investigated: Zr20 ($(\text{Ni}_{0.6}\text{Nb}_{0.4})_{80}\text{Zr}_{20}$), Ta8Zr20 ($(\text{Ni}_{0.6}\text{Nb}_{0.3}\text{Ta}_{0.1})_{80}\text{Zr}_{20}$), Zr30 ($(\text{Ni}_{0.6}\text{Nb}_{0.4})_{70}\text{Zr}_{30}$) and Ta7Zr30 ($(\text{Ni}_{0.6}\text{Nb}_{0.3}\text{Ta}_{0.1})_{70}\text{Zr}_{30}$). The X-ray diffraction patterns were obtained using a PANalytical X'Pert pro θ - θ diffractometer. The ribbons were not coated with Pd. This instrument was equipped with a heating stage with Anton Paar XRK 900. Hydrogen gas was introduced into the heating chamber via a home-made volumetric apparatus. The sample was placed inside the chamber and first evacuated using the turbo pump PFEIFFER model number TSH071E. Simultaneous TGA-DTA measurements were conducted by means of a Setaram Sensys Evolution 1200 TGA system [18] under a high purity argon flux (60 ml/min) at ambient pressure. For each experiment, a sample mass of ~10 mg was used. Different temperature

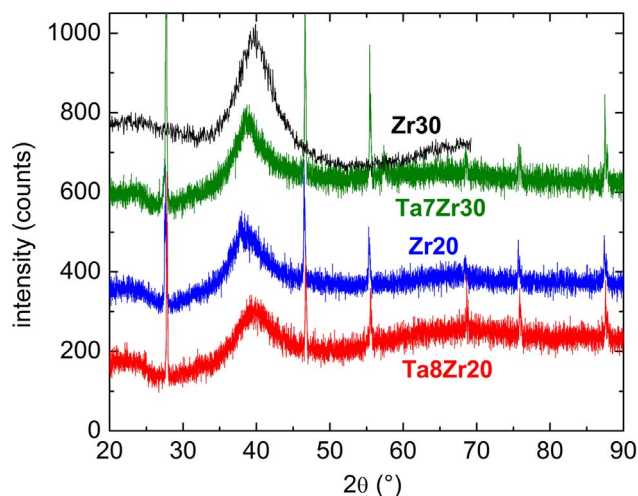


Fig. 1. X-ray diffraction plots of Zr30, Ta7Zr30, Zr20 and Ta8Zr20 samples at room temperature before hydrogen exposure.

rates, between 4 and 20 $^{\circ}\text{C}/\text{min}$, were used for each sample in order to calculate the activation energy of the crystallization process. The hydrogen absorption curves of Zr20, Ta8Zr20 and Ta7Zr30 were recorded by the home-made Sieverts apparatus at Sapienza University of Rome described in Ref. [19,20]. The experiments were performed on specimens with a mass of ~300 mg. For sample Zr30 a different home-made fully automated Sieverts apparatus [21] was used at University of Nevada, Reno.

3. Results and discussion

3.1. X-Ray diffraction measurements on as produced and hydrogenated ribbons

To ascertain whether the ribbons are fully amorphous, we performed X-ray diffraction (XRD) analysis on Zr20, Zr30, Ta8Zr20 and Ta7Zr30. Room temperature XRD patterns were obtained in as-prepared melt-spun condition without any addition of hydrogen (Fig. 1). All the samples showed a broad hump with the highest intensity at 20–38 $^{\circ}$. The crystalline Bragg peaks of Si visible in the spectra of Zr20, Ta8Zr20 and Ta7Zr30 are due to the addition of internal standard sprinkled on the samples. Similar results have been observed by Qiang [22].

In the next set of experiment, we examined the Ta8Zr20 and Ta7Zr30 samples under hydrogen atmosphere at 300–400 $^{\circ}\text{C}$ and 1–10 bar to observe if there are any structural changes. X-ray diffraction results showed the nature of the amorphous material did not change significantly with the addition of hydrogen in the above mentioned conditions (Figs. 2a and b). In case of Ta7Zr30 we even varied the time and did not observe any structural changes (Fig. 2a).

3.2. The crystallization process

A Differential Thermal Analysis apparatus was used to determine the crystallization temperature of Ta added alloys. The crystallization temperature (T_c) of the alloys without any Ta had already been measured in our group; T_c and the activation energies, E_a , of the $(\text{Ni}_{0.6}\text{Nb}_{0.4})_{80}\text{Zr}_{20}$ were 583 $^{\circ}\text{C}$ and 549 kJ/mol, respectively, while for $(\text{Ni}_{0.6}\text{Nb}_{0.4})_{70}\text{Zr}_{30}$ they were $T_c=535$ $^{\circ}\text{C}$ and $E_a=542$ kJ/mol [19,23].

The samples $(\text{Ni}_{0.6}\text{Nb}_{0.4-y}\text{Ta}_y)_{100-x}\text{Zr}_x$ with $y=0.1$ and $x=20, 30$, here investigated for the first time, show more than one exothermic peak (see Fig. 3). In the case of the Ta7Zr30, one can observe two well defined peaks in Fig. 3, while for Ta8Zr20 three peaks are visible (Fig. 3). All of them shift towards higher temperature as the heating rate is increased, indicating a thermally activated character of all

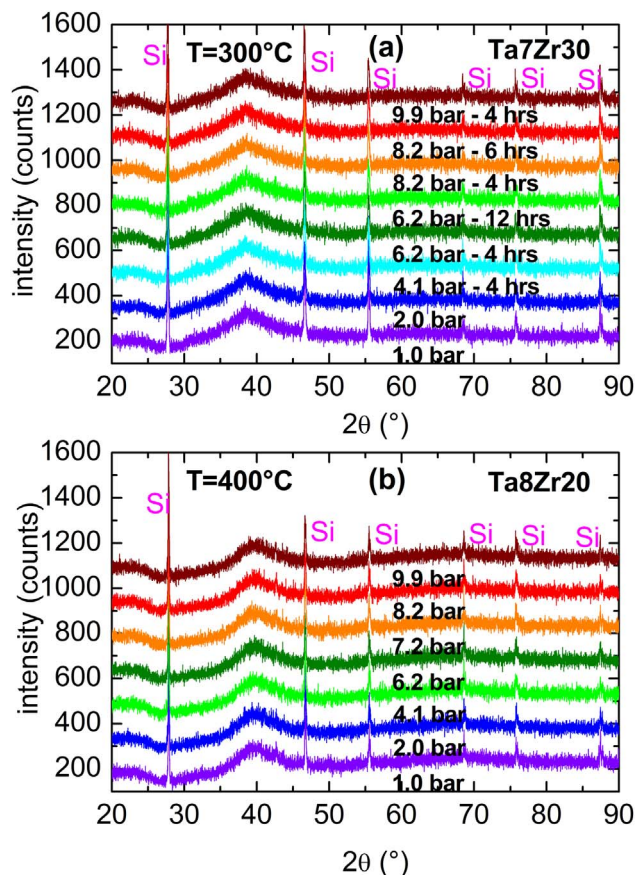


Fig. 2. X-ray diffraction plots of Ta7Zr30 under hydrogen environment of up to ~10 bar at 300 °C (panel a) and of Ta8Zr20 under hydrogen environment of up to ~10 bar at 400 °C.

processes. The fact that one observes more than one peak for the crystallization process is not surprising, as many previous investigations of the crystallization process of amorphous membranes for hydrogen purification reported that it can occur in subsequent steps, as in the present case [2,17,23–25].

In particular, the Ta7Zr30 sample displays a sharp peak which shifts from ~520 to ~540 °C as the temperature rate is varied from 4 to

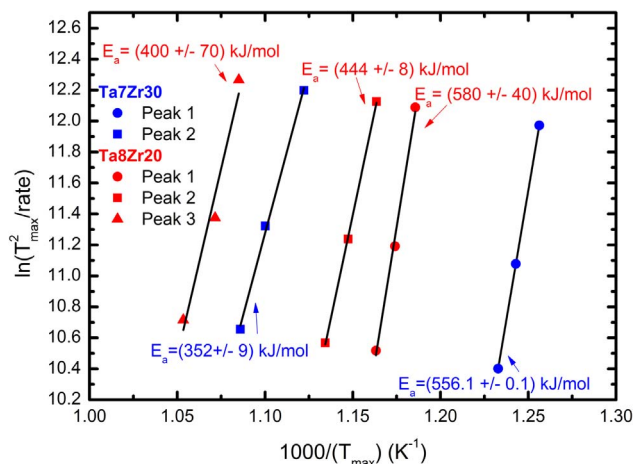


Fig. 4. Kissinger plots for the peaks of the Ta containing samples.

20 °C/min (Peak 1 in panel a of Fig. 3). Moreover, a broader and less well defined peak is present above 600 °C (Peak 2 in panel a of Fig. 3). The DTA traces of Ta8Zr20 show three peaks in the temperature range between 550 and 700 °C (labeled as peak 1, 2 and 3 in Fig. 3, panel b). It must be noted that for all samples the crystallization starts at temperatures higher than 500 °C, a temperature well above the maximum temperature (400 °C) at which the following measurements of hydrogen solubility are conducted, so we can be sure that the samples are in their amorphous state, in agreement with the results of XRD measurements reported in the previous Section.

In order to obtain quantitative information about the activation energy of the subsequent steps of crystallization, we constructed the Kissinger plots [26] for the two peaks of Ta7Zr30 and the three peaks of Ta8Zr20 (Fig. 4). Regarding Ta7Zr30, the Kissinger plot provides a value of $E_a \sim 556.1 \pm 0.1$ kJ/mol for the first process and $E_a \sim 352 \pm 9$ kJ/mol for the second one. In the case of Ta8Zr20 the activation energies of the crystallization steps are found to be 580 ± 40 kJ/mol, 444 ± 8 kJ/mol and 400 ± 70 kJ/mol, respectively for peak 1, 2 and 3. The present measurements confirm that crystallization occurs at lower temperatures as the Zr content is increased [15,17]. Moreover, the activation energies of the Ta containing samples are comparable to those of the Ta free membranes [19,23].

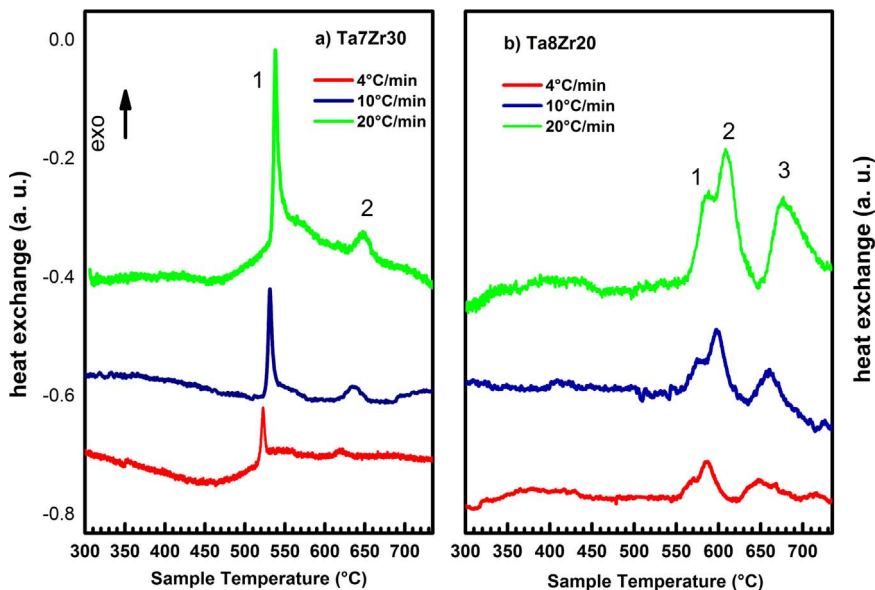


Fig. 3. DTA curves of the Ta containing samples measured at 4, 10 and 20 °C/min.

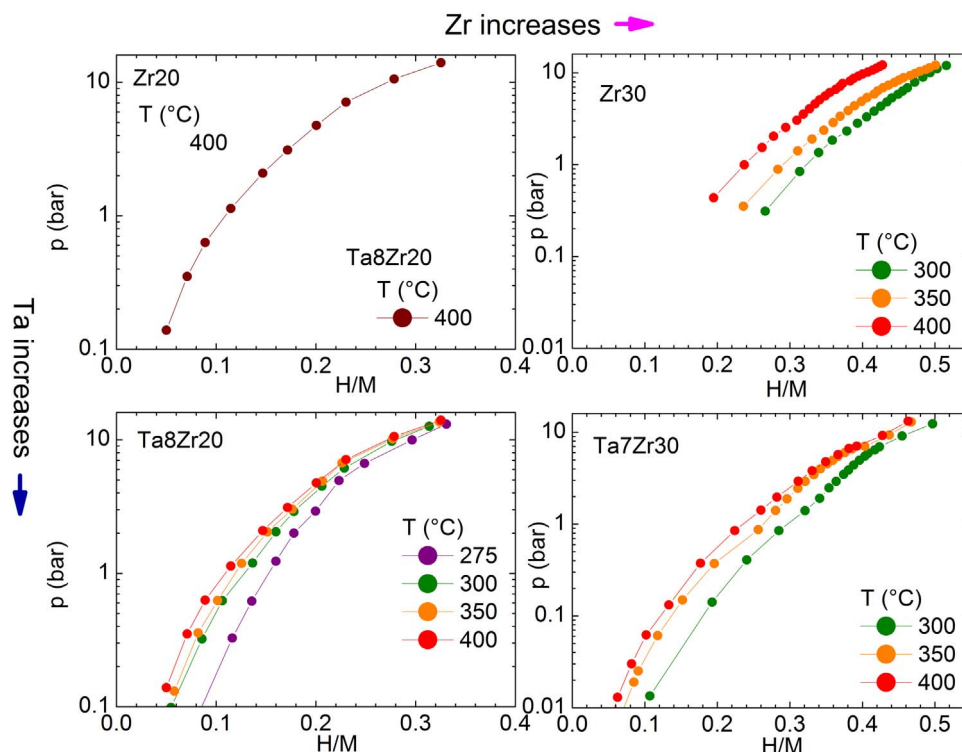


Fig. 5. p-c isotherms of the amorphous membranes.

3.3. Hydrogen solubility

The solubility of hydrogen in the membranes was measured by obtaining pressure – composition isotherms at different temperatures in the range 300–400 °C; these temperatures are well below the crystallization temperature (Fig. 3). The maximum measured pressure was in the range 13–14 bar, as shown in Fig. 5.

One can note in Fig. 5 the absence of pressure plateau with the increasing pressure, as typically observed in crystalline hydrides [27]. In the case of an ideal hydrogen solid solution, hydrogen absorption would be described by the Sieverts law: $X_H = K_H (P_{H_2})^{1/2}$, where X_H is the atomic fraction of hydrogen, P_{H_2} is the equilibrium pressure and K_H the Sieverts law coefficient [28]. In general hydrogen capacity is higher at lower temperature. The plotted square root of pressure vs H/M did not yield a linear relation indicating it does not follow the Sieverts law (results not shown). The absence of any pressure plateau in the isotherms of the amorphous materials has been also theoretically described by means of mean field approximation and Stoner-type condition [29,30]. Other investigators observed the same feature in amorphous $Zr_{60}Al_{10}Ni_{30}$ samples and attributed the absence of pressure plateau to the variation of the site energy of the occupied hydrogen atoms and to the continuous structural changes during hydrogenation [31].

The data for Zr20 alloy membrane showed a very slow kinetics of hydrogenation, possibly due to the oxidation of the surface, and therefore only the p-c isotherm at 400 °C was obtained.

For each membrane, the hydrogen solubility at fixed p decreases as T increases; for example, in the case of Zr30 at the maximum pressure one obtains $H/M \sim 0.52$ for $T=300$ °C and $H/M \sim 0.42$ at $T=400$ °C. At fixed p and T, the hydrogen content is higher in the membranes with a higher Zr content: one obtains a maximum $H/M \sim 0.5$ at 300 °C for Ta7Zr30 and a maximum H/M of ~ 0.33 at the same temperature for Ta8Zr20. Moreover, the curves of the membranes containing the same amount of Zr are close one to the other, when measured at the same temperature.

A direct comparison of the hydrogen absorption properties of the presently studied membranes with previous literature cannot be easily

performed. Indeed, in many cases hydrogenation of Ni-Nb specimen was previously obtained by means of electrolytic charging [32,33]. Only some limited indications from previous papers can be obtained. Indeed, Conic et al. [34] measured the hydrogen absorption in Zr-Nb-Ta alloys in the temperature range between 400 and 700 °C at a hydrogen pressure of 1 bar using the volumetric method and found that the hydrogen concentration decreases as T increases, as in our present study. By means of electrolytic charging, Jayalakshmi et al. [32] attained higher hydrogen content in Ni-Nb-Zr-Ta alloys with a higher concentration of Zr, as in the membranes presently investigated. Similarly Kirchheim et al. [35] and Yamaura et al. [15] reported that in the binary system Ni-Zr the H/M ratio increases with Zr addition; the H/M ratio for our alloy without Ta additions is similar to Yamaura's data [15].

3.4. The hydrogenation enthalpy

In the case of crystalline materials, for which a pressure plateau is observed in the p-c isotherms, one can calculate ΔH_{hyd} from the slope of the van't Hoff plot of $\ln(p)$ vs $1/T$, where p is the plateau pressure at temperature T(K) [36]. However, the pressure-composition isotherms of the presently studied amorphous materials do not exhibit any plateau. In this case, one can estimate the hydrogenation enthalpy, ΔH_{hyd} , from the van't Hoff plots $\ln(p)$ vs $1/T$ at constant values of H/M [36]. In order to obtain the values of p at fixed values of H/M at the various temperatures, an interpolation of the experimental data using beta splines was performed by means of a program implemented with the Labview routines. Fig. 6a shows the van't Hoff plot for Zr30 sample and the best fit curves for H/M values ranging from 0.34 to 0.42 in step of 0.02. Enthalpies vary slightly, from 41 to 33 kJ/mol. A mean value of $\Delta H_{hyd} \sim 37 \pm 4$ kJ/mol is estimated from the hydrogenation absorption measurements for the Zr30 sample. For Ta7Zr30, the hydrogenation enthalpy decreases from 31 kJ/mol at $H/M=0.24$ –27 kJ/mol for $H/M=0.34$. For the Ta8Zr20 membrane, ΔH_{hyd} increases as H/M decreases from ~ 8 kJ/mol at $H/M=0.16$ to ~ 14 kJ/mol at $H/M=0.10$.

It is worth noting that the enthalpy values calculated for Ta8Zr20

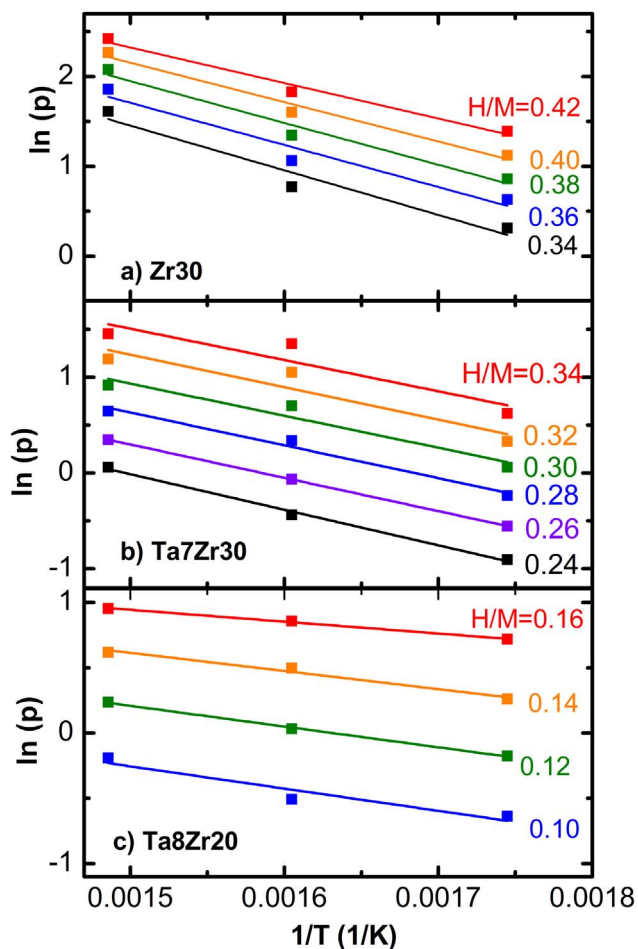


Fig. 6. Van't Hoff plot for samples Zr30 (panel a), Ta7Zr30 (panel b) and Ta8Zr20 (panel c) calculated at different H/M ratios.

are lower than those ones obtained for the samples with higher Zr content, even if they were measured at lower hydrogen concentration. This fact indicates that the hydrogenation enthalpy decreases with the Zr content.

Despite the fact that the absolute values of the hydrogenation enthalpies are different for the samples containing 20 and 30 at% of Zr, one can note that in both cases ΔH_{hyd} decreases as H/M increases. This trend can be related to the different interstitial sites available for hydrogen trapping during the progression of the absorption process: at the beginning the deepest energy levels are occupied, while only shallower energy levels are available at higher hydrogen content. Indeed, Jayalakshmi et al. [18] investigated the thermal desorption process of some Ni-Nb-Zr-Ta amorphous ribbons by means of thermal desorption spectroscopy. These authors [32] linked the dehydrogenation temperature to the energy of the sites occupied by hydrogen atoms: the strongly bonded interstitial sites desorbed at higher temperature than the weakly bonded sites. For samples containing less than 40 at% H, the dehydrogenation occurred above 500 °C, while at higher hydrogen content dehydrogenation started already at 200 °C. These facts suggest that at lower H/M the deeper energy interstitial sites are occupied by H [17], while at higher H/M also the shallower energy levels become populated. The absorption data presently reported [17,32] are consistent with this picture: at higher H/M the hydrogenation enthalpy decreases because the absorption involves the shallower energy sites. The smooth decrease of ΔH_{hyd} as H/M increases suggests that the available interstitial sites form a continuum of energy levels, without jumps in the possible energies.

4. Conclusions

$(\text{Ni}_{0.6}\text{Nb}_{0.4-y}\text{Ta}_y)_{100-x}\text{Zr}_x$ membranes were studied by combining several techniques, which provided indications about their structural and hydrogen absorption properties. The high temperature and elevated pressure structural data for both Ta containing alloys show similar trends under hydrogen atmosphere in the pressure between 1 and 10 bar, and in particular prove that the amorphous structure is maintained also after hydrogenation at 400 °C. The crystallization temperature and the activation energy for crystallization obtained by means of DTA measurements are very similar for Ta-containing and Ta-free sample. The analysis of the volumetric data provides the hydrogenation enthalpies of the samples in their amorphous state. Moreover, they provides indications about the hydrogen occupation sites during hydrogenation, suggesting that at the beginning of the absorption process the deepest energy levels are occupied, while only shallower energy levels are available at higher hydrogen content, with the available interstitial sites forming a continuum of energy sites.

Acknowledgements

This research is supported by the US DOE-NNSA grant number US DE-NA0002004.

References

- [1] S. Sarker, D. Chandra, M. Hirscher, M. Dolan, D. Isheim, J. Wermer, D. Viano, M. Baricco, D. Grant, O. Palumbo, A. Paolone, R. Cantelli, *Appl. Phys. A* 122 (2016) 168.
- [2] S.N. Paglieri, N.K. Pal, M.D. Dolan, S.M. Kim, W.N. Chien, J. Lamb, D. Chandra, K.M. Hubbard, D.P. Moore, *J. Membr. Sci.* 378 (2011) 42–50.
- [3] A. Suzuki, H. Yukawa, T. Nambu, Y. Matsumoto, Y. Murata, *Int. J. Hydrog. Energy* 39 (2014) 7919–7924.
- [4] T.B. Flanagan, D. Wang, S. Luo, *J. Phys. Chem. B* 111 (2007) 10723–10735.
- [5] M. Hara, J. Sakurai, S. Akamaru, K. Hashizume, K. Nishimura, K. Mori, T. Okabe, K. Watanabe, M. Matsuyama, *Mater. Trans.* 48 (2007) 3154–3159.
- [6] E. Serra, M. Kemali, A. Perujo, D.K. Ross, *Metall. Mater. Trans. A* 29 (1998) 1023–1028.
- [7] V.N. Alimov, A.O. Busnyuk, M.E. Notkin, E.Yu. Peredistova, A.I. Livshitsa, *Int. J. Hydrog. Energy* 39 (2014) 19682–19690.
- [8] D. Wang, T.B. Flanagan, K.L. Shanahan, *J. Alloy. Compd.* 349 (2003) 152–163.
- [9] H. Yukawa, D. Yamashita, S. Ito, M. Morinaga, S. Yamaguchi, *Mater. Trans.* 43 (2002) 2752–2762.
- [10] M.D. Dolan, K.G. McLennan, J.D. Way, *J. Phys. Chem. C* 116 (2012) 1512–1518.
- [11] M.D. Dolan, M.E. Kellam, K.G. McLennan, D. Liang, G. Song, *Int. J. Hydrog. Energy* 38 (2013) 9794–9799.
- [12] M.D. Dolan, K.G. McLennan, G. Song, D. Liang, M.E. Kellam, *J. Membr. Sci.* 446 (2013) 405–409.
- [13] J.-H. Shim, W.-S. Ko, K.-H. Kim, H.-S. Lee, Y.-S. Lee, J.-Y. Suh, Y.-W. Cho, B.-J. Lee, *J. Membr. Sci.* 430 (2013) 234–241.
- [14] H. Homma, H. Saitoh, T. Misawa, T. Ohnishi, *Mater. Trans.* 43 (2002) 1110–1115.
- [15] S.-I. Yamaura, M. Sakurai, M. Hasegawa, K. Wakoh, Y. Shimpo, M. Nishida, H. Kimura, E. Matsubara, A. Inoue, *Acta Mater.* 53 (2005) 3703–3711.
- [16] S. Hao, D.S. Sholl, *J. Membr. Sci.* 350 (2010) 402–409.
- [17] M.D. Dolan, N.C. Dave, A.Y. Ilyushechkin, L.D. Morpeth, K.G. McLennan, *J. Membr. Sci.* 285 (2011) 30–55.
- [18] O. Palumbo, A. Paolone, P. Rispoli, R. Cantelli, T. Autrey, *J. Power Sources* 195 (2010) 1615–1618.
- [19] O. Palumbo, S. Brutti, F. Trequattrini, S. Sarker, M.D. Dolan, D. Chandra, A. Paolone, *Energies* 8 (2015) 3944–3954.
- [20] O. Palumbo, F. Trequattrini, F.M. Vitucci, A. Bianchin, A. Paolone, *J. Alloy. Compd.* 645 (2015) S239–S241.
- [21] D. Chandra, A. Sharma, R. Chellappa, W.N. Cathey, F.E. Lynch, R.C. Bowman Jr., J.R. Wermer, S.N. Paglieri, *J. Alloy. Compd.* 452 (2008) 312–324.
- [22] J.B. Qiang, W. Zhang, S. Yamaura, A. Inoue, *Mater. Trans.* 50 (2009) 1236–1239.
- [23] S.-M. Kim, D. Chandra, N.K. Pal, M.D. Dolan, W.-M. Chien, A. Talekar, J. Lamb, S.N. Paglieri, T.B. Flanagan, *Int. J. Hydrog. Energy* 37 (2012) 3904–3913.
- [24] M.D. Dolan, S. Hara, N.C. Dave, K. Haraya, K. Ishitsuka, A.Y. Ilyushechkin, K. Kita, K.G. McLennan, L.D. Morpeth, M. Mukaida, *Sep. Purif. Technol.* 65 (2009) 298–304.
- [25] M.D. Dolan, N. Dave, L. Morpeth, R. Donelson, D. Liang, M. Kellam, S. Song, *J. Membr. Sci.* 326 (2009) 549–555.
- [26] H.E. Kissinger, *He. Anal. Chem.* 29 (1957) 1702–1706.
- [27] Y. Fukai, 2nd rev. *The Metal-Hydride System, Basic Bulk Properties* 21, Springer Series in Materials Science, 2005.
- [28] S. Hara, M. Ishitsuka, H. Suda, M. Mukaida, K. Haraya, *J. Phys. Chem. B* 113 (2009) 9795–9801.
- [29] R. Griessen, *Phys. Rev. B* 27 (1983) 7575–7582.

- [30] P.M. Richards, Phys. Rev. B 30 (1984) 5183–5189.
- [31] X.G. Li, T. Otahara, S. Takahashi, T. Shoji, H.M. Kimura, A. Inoue, J. Alloy. Compds. 297 (2000) 303–311.
- [32] S. Jayalakshmi, Y.G. Choi, Y.C. Kim, Y.B. Kim, E. Fleury, Intermetallics 18 (2010) 1988–1993.
- [33] S. Jayalakshmi, V.S. Vasantha, E. Fleury, M. Gupta, Appl. Energy 90 (2012) 94–99.
- [34] D. Conic, A. Gradisek, J. Radakovic, M. Iordoc, M. Mirkovic, M. Cebela, K. Batalovi, Int. J. Hydrog. Energ. 40 (2015) 5677–5682.
- [35] R. Kirchheim, W. Kieninger, X.Y. Huang, S.M. Filipek, J. Rush, T. Udovic, J. Less-Common Met. 172–174 (1991) 880–889.
- [36] B.L. Karger, L.R. Snyder, C. Horvath, An Introduction to Separation Science, Wiley, New York, 1973.